Bulk meltwater flow and liquid water content of snowpacks mapped with the electrical self-potential (SP) method

S. S. Thompson[1, *], B. Kulessa[2], R. L. H. Essery[3], M. P. Lüthi[4, *]

(1) Department of Arctic Geology, University Centre in Svalbard (UNIS), Svalbard

(2) College of Science, Swansea University, UK

(3) The School of Geosciences, University of Edinburgh, UK

(4) University of Zurich, Switzerland

(*) Formerly at Versuchsanstalt für Wasserbau, Hydrologie und Glaziology (VAW), ETH Zürich, Switzerland

Correspondence to S. S. Thompson (Sarah.Thompson@unis.no)

ABSTRACT

Our ability to measure, quantify and assimilate hydrological properties and processes of snow in operational models is disproportionally poor compared to the significance of seasonal snowmelt as a global water resource and major risk factor in flood and avalanche forecasting. We show here that strong electrical self-potential fields are generated in melting in-situ snowpacks at Rhone Glacier and Jungfraujoch Glacier, Switzerland. In agreement with theory the diurnal evolution of self-potential magnitudes (~ 60 – 250 mV) relates to those of bulk meltwater fluxes ($0 – 1.2 \times 10^{-6}$ m^3 s^{-1}) principally through the permeability and the content, electrical conductivity (EC) and pH of liquid water. Previous work revealed that when fresh snow melts, ions are eluted in sequence and EC, pH and self-potential data change diagnostically. Our snowpacks had experienced earlier stages of melt, and complementary snow pit measurements revealed that EC (~ $1\text{-}5 \times 10^{-6}$ S m^{-1}) and pH (~ 6.5 –

6.7) as well as permeabilities (respectively ~ 9.7 $\times 10^{-5}$ m^2 and ~ 4.3 $\times 10^{-5}$ m^2 and Rhone Glacier and Jungfraujoch Glacier) were invariant. This implies, first, that preferential elution of ions was complete and, second, that our self-potential measurements reflect daily changes in liquid water contents. These were calculated to increase within the pendular regime from ~ 1 – 5 % and ~ 3 – 5.5 % respectively at Rhone Glacier and Jungfraujoch Glacier, as confirmed by ground truth measurements. We conclude that the electrical self-potential method is a promising snow and firn hydrological sensor owing to its suitability for [1] sensing lateral and vertical liquid water flows directly and minimally invasively, [2] complementing established observational programs through multidimensional spatial mapping of meltwater fluxes or liquid water content, and [3] low-cost autonomous monitoring. Future work should focus on the development of self-potential sensor arrays compatible with existing weather and snow monitoring technology and observational programs, and the integration of self-potential data into analytical frameworks.

1. Introduction

More than a sixth of the world's population relies on melt from seasonal snow and glaciers for water supply (Barnett et al., 2005). Snow, and runoff from snow, are also major resources for the hydroelectric, tourism and inland fishery industries, and furthermore represent hazards from flooding and avalanches (Mitterer et al., 2011). The availability of snow models constrained by a reliable observational basis, for the forecasting of snow hydrological properties and processes in climate, resource and hazard applications is therefore of considerable socio-economic significance (Wever et al., 2014). However, the parameterisation of fundamental snow-hydrological attributes, such as liquid water content and flux, is a well-recognised major source of uncertainty in operational models used in snow and hydrological forecasting (Livneh et al., 2010, Essery et al., 2013). This uncertainty in

operational models is rooted principally in the inability of traditional snow-hydrological techniques to provide automated attribute measurements non-invasively and on spatial scales that match those used in operational snow models. Relevant traditional techniques include dielectric (Denoth, 1994) or 'hand' tests (Fierz et al., 2009) of snow liquid water contents, lysimeter measurements of discharge, temperature and pH and electrical conductivity of bulk meltwaters (Campbell et al., 2006, Williams et al., 2010), and manual observation or measurement of snow density and grain size (Fierz et al., 2009). Even cutting edge upward-looking radar measurements of snowpack structure and liquid water content (Heilig et al., 2010; Mitterer et al., 2011; Schmid et al., 2014) compare unfavourably with model predictions of wetting front propagation (Wever et al., 2014), attributed to inherent limitations of 1-D approach in capturing preferential flow.

By combining field measurements with a theory and model of self-potential signals associated with unsaturated flow in melting snow (Kulessa et al. 2012), we show here that electrical self-potential geophysical data integrated with traditional snow measurements can address these limitations. The self-potential technique is a passive geo-electrical method that exploits the presence of naturally-occurring electrical potentials in the subsurface generated as a result of dipolar charge separation when water flows through a porous matrix ('streaming potential'; Darnet et al., 2003, Revil et al., 2006). The self-potential method has a unique ability in delineating, monitoring, and quantifying the flow of subsurface water in groundwater aquifers and unsaturated media (e.g., Revil et al., 2006, and references therein), and for numerous cold regions application (e.g., French et al., 2006; Kulessa, 2007, and references therein). This ability is due on the fact that pore waters generally have an excess of electrical charge due to the electrical double layer at the interface between the solid matrix (in this case snow grains) and pore water. The advective drag of this excess of electrical charge is responsible for a streaming current, whose divergence generates a quasistatic electric field

known as the streaming potential (Sill, 1983; Revil et al., 2003). More recently, streaming potential theory has been extended for unsaturated conditions (Linde et al., 2007; Revil et al., 2007; Jougnot et al., 2012). A new theory and numerical model of self-potential signals associated with unsaturated flow in melting snow, along with laboratory tests, strongly promoted the technique as a non-intrusive hydrological sensor of water fluxes (Kulessa et al., 2012) at spatial scales intermediate between snow pits and satellite footprints or, given independent flux measurements, of evolving physical and chemical properties of snow and snow-melt.

We answer two fundamental questions: 1) Can the self-potential method serve as a non-intrusive field sensor of temporally evolving bulk meltwater fluxes and liquid water contents of snow? 2) What are the ambiguities introduced into estimates of liquid water contents from self-potential and bulk discharge data, by uncertainties inherent in the governing snow physical and chemical properties? Lastly we discuss the implications and possibilities of the technique for future snow measurement and modelling research and practice. Our study thus takes a significant step towards the in-situ implementation of the self-potential method for improved characterization and monitoring of snow liquid water contents and melt water fluxes.

2. Theory, field sites and methods

The Poisson equation relates the electrical field ψ to the source current density in a partially or fully-saturated snow pack,

$$\nabla \cdot \left(\sigma \nabla \psi \right) = \nabla \cdot \mathbf{j}_S , \tag{1}$$

where σ is the bulk electrical conductivity of the porous material (in S m^{-1}), and $\mathbf{j}_S$ is the source current density (in A m^{-2}). Equation (1) applies only in the low-frequency limit of the Maxwell's equations without external injection or retrieval of charges, or charge storage in the snowpack. Extending the classic Helmholtz-Smoluchowski theory for unsaturated flow in snow, the one-dimensional solution to equation (1) is given by

$$\psi_m - \psi_0 = -\frac{\varepsilon\zeta}{\eta\sigma_w} S_w (H_m - H_0), \tag{2}$$

where ψ_m and H_m are respectively the electrical and hydraulic potentials at the measurement electrode, ψ_0 and H_0 are the corresponding potentials at the reference electrode, ζ is the zeta potential (V), and ε, η, σ_w and S_w are respectively the dielectric permittivity (F m^{-1}), dynamic viscosity (in Pa s), electrical conductivity (S m^{-1}) and relative saturation (dimensionless) of the melt or rainwaters in the snowpack's pore space (Kulessa et al., 2012). The zeta potential is the voltage across the electrical double layer at the interface between the ice matrix and the pore waters, as controlled by these constituents' physical and electrical properties.

To address the specific objectives set out in the introduction through data-driven testing, we developed an experimental survey design to simulate the geometry of Kulessa et al.'s (2012) laboratory snow column (Fig. 1b). It was therefore our aim to characterise lateral bulk meltwater fluxes in inclined snowpacks at two glaciers in Valais, Switzerland, measuring all relevant snow pack attributes for ground truth. Self-potential and traditional snow-hydrological measurements were acquired on 13th, 14th and 15th June 2013 from the ablation area snowpack at Rhone Glacier, and 5th September 2013 from the glacial accumulation area at Jungfraujoch Glacier (Fig.1a). At Rhone Glacier and Jungfraujoch

120 Glacier site elevations were respectively 2340 and 3460 m.asl., with surface gradients of ~ 8°
121 and 17°. At the Rhone Glacier all three days experienced comparable air temperature,
122 although 15th June was noticeably cloudier with a very low sunshine duration. Because daily
123 average temperatures were between 5 and 15 °C with no fresh snowfall (MeteoSuisse), the
124 snowpacks would have experienced significant melting in the weeks before the surveys. We
125 therefore expect them to be physically mature in terms of enhanced grain size and density due
126 to metamorphosis, and chemically mature in terms of invariant meltwater pH and electrical
127 conductivity as preferential elution of solutes has been completed (Kulessa et al., 2012, and
128 references therein).

129 At both sites more than 100 self-potential measurements were made at the snow
130 surface, and meltwater bulk discharge in a lysimeter, pH and electrical conductivity, and
131 snowpack characteristics including thickness, density, grain size and liquid water content
132 were recorded. Adopting our established acquisition procedures (Thompson et al., 2012), we
133 conducted all self-potential surveys using a pair of lead/lead chloride 'Petiau' non-polarising
134 electrodes (Petiau, 2000). The survey was carried out following the potential amplitude
135 method (Corry et al., 1983); this employs a reference electrode in a fixed location and a
136 roving electrode which is moved through the survey area at 0.5 m intervals (Fig.1a). Self-
137 potential surveys were conducted in profiles of 25 data points perpendicular to the principal
138 direction of water flow, where the latter was assumed to follow the gradient indicated by
139 snow surface topography. All self-potential measurements were taken as differential readings
140 relative to the reference electrode, minimizing streaming, electrochemical and thermal
141 potentials at the latter by grounding them outside the survey areas (Fig. 1a), submerged in a
142 glass jar, open at the top and filled with water-saturated local media (Kulessa et al., 2003a).
143 The jar was then buried upright ~1 m deep to avoid exposure to surface temperature
144 variations. Surveys were carried out with a fixed tie-in point (measured every second line) at

145 the reference electrode, allowing for correction of the effects of electrode polarisation and
146 drift (Doherty et al., 2010, Thompson et al., 2012).

147 Bulk discharge through a snowpack is preferably measured with a lysimeter
148 (Campbell et al., 2006, Williams et al., 2010), in this case made up of a series of smaller
149 (guttering) areas joined together to prevent freezing and compaction (after Campbell et al.,
150 2006). The lysimeter was placed at the base of Rhone Glacier's snowpack, and at the limit of
151 the diurnal melt penetration depth at Jungfraujoch Glacier (determined by daily dye tracing
152 experiments). Snow density (by balance) and average snow grain size (crystal card and lens)
153 were measured, at the start and end of each self-potential survey to reveal any intermittent
154 snow metamorphism, using standardised techniques within the top and basal layers of snow
155 pits freshly excavated at the survey sites (Fierz et al., 2009). Liquid water content was
156 estimated using two different techniques, including the hand test (Colbeck et al., 1990, Fierz
157 et al., 2009) in the surface and base layers of Rhone Glacier's snow pit, and the Denoth
158 Capacitance Meter (Denoth, 1994) in the surface and base layers of the snow pit at
159 Jungfraujoch Glacier. The latter were acquired across a 2D grid where the instrument was
160 inserted into the snowpack at a depth of 0.4 m following the same survey spacing as the self-
161 potential measurements.

162

163 **3. Field measurement results**

164 The drift-corrected self-potential magnitudes and meltwater bulk discharges both increase
165 with time through the day until a peak in late afternoon, after which they both begin to
166 decrease (Fig. 2). There is no distinguishable time lag between the measured self-potential
167 magnitude and discharge data (Fig. 2), and the ratio between self-potential and bulk discharge
168 changes consistently over time (Fig.3). Days 1 and 2 at Rhone Glacier were characterised by
169 higher discharges and self-potential magnitudes compared to day 3, and intriguingly bulk

discharge at Jungfraujoch Glacier was akin to day 3 at Rhone Glacier but self-potential magnitudes at Jungfraujoch Glacier were much higher than days 1 and 2 at Rhone Glacier (Fig. 2). The pH, electrical conductivity and temperature of meltwater, recorded with each bulk discharge measurement, show no consistent temporal or spatial variation across any of the four field surveys. Fluid electrical conductivity values generally ranged between 1×10^{-6} S m^{-1} and 5×10^{-6} S m^{-1} without spatial or temporal consistency, while pH ranged between 6.5 and 6.9. Snow grain size remained constant at ~ 1.5 mm at Rhone Glacier and ~ 1 mm at Jungfraujoch Glacier, while snow densities ranged between 555 kg m^{-3} and 573 kg m^{-3} without spatial or temporal consistency. The very small variability range of the snowpack characteristics measured is consistent with mature snowpacks, as assumed above with reference to prior meteorological conditions. At Rhone Glacier the liquid water content of snow had a wetness index of 3 irrespective of measurement time or location at the surface or base of the snow pit, associated with a liquid water content range of 3 – 8 % vol. (Colbeck et al., 1990). At Jungfraujoch Glacier liquid water content, measured using the Denoth meter, gave profile-averaged values of 1.5 to ~5.0 % vol., increasing consistently throughout the survey period. These measurements and inherent uncertainties are used below for snow liquid water content calculations, uncertainty analysis and sensitivity testing.

4. Objective 1: Self-potential as a snow-hydrological sensor

Both survey areas were south facing, topographically-inclined but otherwise had no visibly distinguished snow surface undulations, and any snow thickness variations were minimal. We therefore expect changes in self-potential magnitudes to be pronounced in the downslope direction, and minimal across-slope along any individual profile (Fig. 1a). Averaging all 25 self-potential data points acquired along any particular profile, a one-dimensional upslope-downslope series of self-potential magnitudes is produced for a given survey area on a given

195 day, together with uncertainty estimates reflecting natural spatial and temporal variability
196 along the profile (Supporting Information). For each profile the acquisition time of the central
197 data point was assigned to it, and all measurements of snowpack and meltwater properties
198 were averaged over the same time period (~ 20 mins, i.e. the acquisition time of any one self
199 -potential profile). The upslope-downslope series of average self-potential magnitudes thus
200 emulates measurements along a horizontally inclined version of the one-dimensional snow
201 column used in Kulessa et al. (2012) (Fig. 1b). These authors reformulated the one-
202 dimensional solution in equation (2) to relate measured self-potential magnitudes and bulk
203 discharges through their partially saturated snow column, which we can therefore adapt here
204 to our field experiment.

205 This adaptation is dependent on four key assumptions, including; 1) water flow within
206 the survey areas' snowpacks is laminar and homogenous in three dimensions, where
207 snowpack surface and base have constant and equal inclination and thus maintain a spatially
208 constant hydraulic gradient; 2) all contributions to the measured self-potential signal from
209 flow below the base of the snowpack, runoff at the surface of the snowpack, and flow outside
210 the lateral boundaries of the survey areas' snowpacks are negligible, and all water
211 contributing to the measured self-potential signals is adequately captured by our bulk
212 discharge measurements; 3) all snow physical and chemical properties controlling the self-
213 potential magnitude do not vary spatially across the survey areas' snowpacks, so that our
214 ground-truth snow-pit data apply uniformly across them, and 4) any spatial changes in self-
215 potential magnitudes are dominated by temporal changes in snow or meltwater properties,
216 while static elevation driven spatial changes are negligible. We assess the implications of any
217 potential violations to these assumptions in Section 6.

218 At a given time, t_n, the measured self-potential field, $\Psi_m(t_n)$, in our survey area is the
219 difference between the locally produced self-potential field, $\Psi_l(t_n)$, and the self-potential field

at the reference electrode, $\Psi_0(t_n)$. The latter is unknown in our field feasibility study, although our method of emplacing the reference electrode is elaborate and designed to eliminate, or at least minimise, any streaming potentials at the reference electrode. Once the reference electrodes have settled in their environments, we further expect any electrochemical or thermal potentials to be negligible. We can therefore expect $\Psi_0(t_n)$ to be close to zero, but nonetheless apply caution and take a two-step approach. Initially we eliminate the reference self-potential fields by considering temporal changes in measured self-potentials only before, subsequently, considering absolute self-potential magnitudes.

Temporal changes in self-potential magnitudes.

We can eliminate the reference field by differencing two self-potential measurements acquired at two successive times:

$$\psi_m(t_n) - \psi_m(t_{n-1}) = \psi_l(t_n) - \psi_l(t_{n-1}) \tag{3}$$

Equation (3) assumes that Ψ_0 and H_0 are temporally invariant, a reasonable supposition for drift-corrected self-potential data if the reference electrode is correctly emplaced. Recognising that $\psi_0 = H_0 \approx 0$ for their snow column experiment, Kulessa et al. (2012) reformulated equation (2) to show that the self-potential field at a measurement electrode, $\Psi_l(t_n)$, can be approximated by

$$\psi_l(t_n) = \frac{\varepsilon\zeta}{\sigma_w} \frac{S_w(t_n)}{S_e^n(t_n)} \frac{1}{kA} Q(t_n) \tag{4}$$

where Q ($m^3\ s^{-1}$) is bulk discharge in the snow pack through cross-sectional area A (m^2), k is permeability, S_e is effective saturation and $n \approx 3.3$ is the saturation exponent (after Albert et al., 1998, Kulessa et al., 2012). Assuming that any temporal changes in the self-potential field at the reference electrodes in our field experiments are negligible, the difference between successive field self-potential measurements in time can be approximated by

$$\psi_m(t_n) - \psi_m(t_{n-1}) = \frac{\varepsilon\zeta}{\sigma_w}\frac{1}{kA}\left(\frac{S_w(t_n)}{S_e^n(t_n)}Q(t_n) - \frac{S_w(t_{n-1})}{S_e^n(t_{n-1})}Q(t_{n-1})\right). \quad (5)$$

In the present case we have measured $\Psi_m(t_n)$ and $\Psi_m(t_{n-1})$ as well as $Q(t_n)$ and $Q(t_{n-1})$. We have also measured, or can estimate from well-established empirical relationships, all other parameters coupling the temporal difference in self-potential fields ($\Psi_m(t_n)$ and $\Psi_m(t_{n-1})$) to that of discharge (expression in the large parentheses on the right-hand side of equation(5)). To demonstrate the usefulness of self-potential measurements in snow research and practice, we can therefore evaluate equation (5) at successive times, t_n and t_{n-1}, to calculate temporal changes in the liquid water content, S_w, of the snowpacks at our field sites. This evaluation is subject to assumptions (1) to (4) above, and is ground-truthed using snow pit measurements of liquid water contents.

At both Rhone Glacier and Jungfraujoch Glacier self-potential magnitude (Ψ_m), bulk discharge (Q), electrical conductivity (σ_w) and cross-sectional area (A) (survey area width × snow depth) were measured directly. Assuming that water at 0 °C has a dielectric permittivity of $\varepsilon_r = 88$, the dielectric permittivity (F m^{-1}) of pore meltwater is $\varepsilon = \varepsilon_r\varepsilon_0 = 7.8 \times 10^{-9}$ F m^{-1}, where $\varepsilon_0 = 8.85 \times 10^{-12}$ F m^{-1} is the dielectric permittivity of vacuum. Permeability (k) can be derived from our snow density (ρ_s) and grain size (d) measurements using Shimizu's (1970) empirical relationship

$$k = 0.077 d^2 e^{-0.0078\rho_s} \quad (6)$$

where k is in m^2, d is in m and ρ_s in kg m^{-3}. This commonly used equation was derived from a fit to laboratory data collected with small rounded grains and a starting grain diameter of ~0.33 mm (Shimizu, 1970). However, later work ascertained experimentally that Shimizu's [1970] empirical formula does in fact apply to a much larger range of grain diameters, as expected to be encountered in practice (less than 0.33 mm to greater than 2 mm) (Jordan et al., 1999). We can therefore expect equation (6) to be robust for our purposes. Effective saturation (S_e) and S_w are related through the irreducible water saturation S_w^{ir} by

$$S_e = \frac{S_w - S_w^{ir}}{1 - S_w^{ir}} \quad (7)$$

In the absence of direct measurements we adopt the commonly used values of $S_w^{ir} = 0.03$ and $n \approx 3.3$ (Kulessa et al., 2012), and assume that these values are invariant in space and time at our study sites.

A significant challenge arises however in that there is one remaining parameter, the zeta potential (ζ), which is unknown here and poorly constrained in general. Earlier work on artificial ice samples, of fixed bulk electrical conductivity, ascertained that the zeta potential reverses sign from ~ +0.01 V to ~ -0.02 V as equilibrium pH increases from less than 3 to greater than 8 (Drzymala et al., 1999, Kallay et al., 2003). The electrochemical properties of the electrical double layer at the snow grain surfaces, and thus also the magnitude and potentially the sign of the zeta potential, will change over time in a fresh snowpack as the snow is affected by melt, recrystallisation and the preferential elution of ions (Meyer and

Wania, 2008, Meyer et al., 2009, Williams et al,. 1999). Recent 'natural snowmelt' laboratory experiments were consistent with a progressive increase of pH from 4.3 to 6.3 and a simultaneous decrease in electrical conductivity from ~ 1×10^{-1} S m^{-1} to ~ 6×10^{-7} S m^{-1}, as the elution of ions follows a well-known sequence (Kulessa et al., 2012)). Upon conclusion of the Kulessa et al.'s (2012) laboratory experiments, modelled rates of change of pH and electrical conductivity were minimal and the snow column mature. The zeta potential is principally a function of pH and electrical conductivity

$$\zeta(\sigma_w, pH) = [\alpha + \beta log_{10}\sigma_w]\left(sin\frac{\pi}{12}[pH_w - pH_w(pzc)]\right), \quad (8)$$

where α and β depend on the chemical composition of the pore fluid and can be determined empirically (Revil et al., 1999). Kulessa et al. (2012) inferred the zeta potential changed from ~ -7.5×10^{-2} V at the start of the natural snowmelt experiments to $+1.5 \times 10^{-2}$ V at the end, when the rate of change of the zeta potential was minimal.

The final values of pH and electrical conductivity that Kulessa et al. (2012) calculated from equation 8 were similar to those measured at Rhone Glacier and Jungfraujoch Glacier (respectively ~ 6.5 – 6.9 and ~ $1 – 5 \times 10^{-6}$ S m^{-1}), suggesting that these in-situ snow packs were likewise mature as expected (Section 2). This inference is corroborated by the absence of consistent spatial or temporal changes in either pH or electrical conductivity throughout the survey periods. In Kulessa et al.'s (2012) laboratory study, the pH-corrected zeta potential had values around zero for the range of electrical conductivities ($1 – 5 \times 10^{-6}$ S m^{-1}) measured at Rhone Glacier and Jungfraujoch Glacier ($1 – 5 \times 10^{-6}$ S m^{-1}), and its rate of change became minimal along with those of pH and electrical conductivity. We can therefore expect a small and invariant zeta potential value to apply to the snowpacks at Rhone Glacier and Jungfraujoch Glacier. Indeed, an excellent fit ($R^2 \approx 0.85$) between liquid water contents

310 measured at Jungfraujoch Glacier with the Denoth meter and that calculated based on
311 equation (5) is obtained when the zeta potential is assigned a value of ~ -1×10^{-5} V (Fig. 4).
312 This excellent fit suggests that in-situ measurements or empirically derived estimates of the
313 parameters affecting coupling between measured self-potential magnitudes and discharges in
314 equation (5) are robust for practical purposes.
315
316 ***Absolute changes in self-potential magnitudes***.
317 The same parameters affect the coupling between temporal changes in self-potential
318 magnitudes and discharge (equation 5), and absolute changes therein as described by
319 equation (4) derived by assuming that the reference potential is zero. We are therefore
320 encouraged to calculate absolute liquid water contents from our self-potential data using
321 equation (4). We do this initially for Jungfraujoch Glacier because here we have detailed
322 ground-truth measurements of liquid water content made with a Denoth meter. Encouragingly
323 we find that calculated and measured ground-truth data match each other very well (Fig. 5a),
324 attesting to the fact that the reference potentials at Jungfraujoch Glacier may not only be
325 temporally invariant as confirmed earlier, but generally have negligible magnitudes.
326 We can apply the same expectation of negligible reference self-potential magnitudes
327 to our surveys at Rhone Glacier on the three successive days. We find that absolute liquid
328 water contents inferred from equation (4) generally fall well within the range of ~ 3 – 8%
329 inferred from our ground-truth hand tests. We can therefore conclude that given careful
330 emplacement of the reference electrode, the simple empirical relationship between self-
331 potential magnitudes, discharge and liquid water content is robust not only in a laboratory
332 setting (Kulessa et al., 2012), but also for application to in-situ snowpacks. The self-potential
333 method therefore shows considerable promise as a non-intrusive snow-hydrological sensor.
334

5. Objective 2: Self-potential sensitivity to uncertainty in snow properties

We evaluate the sensitivity of calculated liquid water contents to both individual and combined parameter uncertainties. For each parameter a range of uncertainty values was created, with the respective minima and maxima approximately twice that of the uncertainty (Table 1). Repeat water content calculations were carried out initially by changing each parameter individually for a range of values between the respective minima and maxima. The results cluster broadly in three categories, including the zeta potential (up to ~ 20 % change in liquid water content within the 50 % uncertainty range), followed by grain diameter, survey area width, electrical conductivity, snow depth and snow density (~ 3 – 4 % change) and bulk discharge, and self-potential (2 % change) (Fig. 6). These three categories readily reflect our knowledge of or ability to measure in-situ the respective parameters, with surprisingly low sensitivity to cross-sectional area despite our simplistic calculation and significant inherent assumptions (i.e. 1 – 4 in Section 4). Self-potential magnitudes are readily measured in the field with minimum uncertainty (Fig. 6), although the strongly enhanced sensitivity to the zeta potential highlights the need for focused research to tightly constrain possible values of this parameter in in-situ snow packs.

While this gives a good indication of the parameters to which water content calculations are most sensitive, it does not indicate possible feedbacks between parameters. Feedbacks were therefore evaluated by calculating liquid water contents for all possible combinations of the best estimates and minimum and maximum parameter values (Table 1), giving over 6500 solutions (Fig. 7). The minimum and maximum outputs were then adopted as the lower and upper uncertainty bounds (Fig.3). Due to the large potential uncertainty in the zeta potential, the sensitivity range was arbitrarily set to ± 50 % for illustrative purposes (Section 4).

Despite our consideration of extreme potential error bounds, calculated uncertainties in liquid water contents are restricted to a relatively small range (~ 20 % for large assumed uncertainty in the zeta potential, and ~ 3 – 4 % otherwise) at both Rhone Glacier and Jungfraujoch Glacier, and absolute values remain within the pendular regime where water bodies in the pore space remain isolated. At the latter site the daily evolution of liquid water contents thus is well captured even if uncertainty is taken into account (Fig. 5b), and likewise at Rhone Glacier calculated liquid water contents plus uncertainties still fall within the range of field measurements (Fig. 5a). Our inferences thus not only support Kulessa et al.'s (2012) notion that existing snow hydrological relationships are robust for modelling purposes, but also suggest that they may apply to in-situ field surveys. These inferences can also provide an explanation for the relatively large self-potential magnitudes generated by relatively low bulk discharge at Jungfraujoch Glacier (Fig. 2). Because we did not observe or infer any consistent or statistically-significant differences between Rhone Glacier and Jungfraujoch Glacier in dielectric permittivity (ε), zeta potential (ζ), saturation ($S_w\ S_e^{-n}$), electrical conductivity (σ_w) or cross-sectional area (A), the only remaining parameter that could facilitate the observed relative difference is permeability (k). Indeed, using an average snow density of 564 kg m^{-3}, the differences in mean snow grain sizes between Rhone Glacier (1.5×10^{-3} m) and Jungfraujoch Glacier (1×10^{-3} m) translate into respective permeabilities of 9.7×10^{-5} m^2 and 4.3×10^{-5} m^2. The relatively reduced permeability of Jungfraujoch Glacier's accumulation-area snow-pack therefore likely supported the presence of self-potential magnitudes that were markedly elevated relative to Rhone Glacier's ablation-area snow-pack (equation (4)). This inference emphasises the sensitivity of the self-potential method to permeability as a fundamental snow-hydrological property, along with its observed sensitivity to bulk melt water discharge and inferred sensitivity to liquid water content.

6. Synthesis and conclusions

The ability of the electrical self-potential method to sense meltwater flow in in-situ snowpacks is unique, where self-potential magnitudes scale directly with discharge and are zero in the absence of flow. The scaling factor depends principally on the liquid water content of the snowpack, its permeability and the water chemistry (Kulessa et al., 2012). We have shown here that diurnal variations in the liquid water content of in-situ snowpacks can be derived from electrical self-potential data and bulk discharge measurements with a simple lysimeter. This derivation was subject to four key assumptions (Section 4) which we now examine in turn to identify what, if any, constraints arise for future applications.

The Reynolds number (*Re*) is a common measure of the mode of fluid flow through porous media, as discussed in a relevant cryospheric context by Kulessa et al. (2003a)

$$Re = \frac{\rho_s v L}{\eta} \tag{9}$$

where v and L are respectively characteristic fluid flow velocity (in m s^{-1}) and characteristic length scale of flow (in m), and ρ_s and η are respectively snow density (in kg m^{-3}) and dynamic viscosity (in Pa s). To a first approximation the transition from laminar to turbulent flow nominally occurs when $Re \approx 10$, although laminar flow can persist at much higher values of *Re* (for comparison, in open channels transition occurs at $Re \approx 2300$). For our purposes *v* can be assumed to correspond to the average linear velocity of flow, $v = Q A^{-1} n^{-1}$, where n is effective porosity (ratio of snow and ice densities). In porous media such as snow L corresponds to the average pore diameter, and in the absence of direct evidence is assumed to be equal to grain size; in practice an overestimation of pore diameter. For the respective snow properties and their uncertainties reported in Table 1 values of Re between ~ 0.1 and ~ 50.7 are obtained, with a best estimate of $Re \approx 1.1$. These values pertain to times of highest

408 measured meltwater discharge when the Reynolds number is likely be greatest. Despite the
409 unrealistically large uncertainty bounds considered in Table 1, and the overestimation of pore
410 diameter (L) and associated inflation of the Reynolds number (equation (9)), we can therefore
411 conclude that meltwater flow in our snowpacks was laminar. The absolute and relative
412 inclinations of the snow surface and base will vary to different degrees within different field
413 areas, thus generating differences in discharge and potentially preferential flow. Indeed, it is
414 an exciting attribute of self-potential measurements that they will, in practice, aid to delineate
415 such differences in meltwater flow.

416 Persistent meltwater runoff at the snow surface is uncommon, and meltwater flow
417 through underlying soils or ice will normally be negligible or small compared to flow through
418 or at the base of snowpacks. We have also shown that the inversion of self-potential data for
419 snow properties such as liquid water content is insensitive to the area of snowpack
420 contributing meltwater flow to the measured signals. Uncertainties in the area of origin of
421 water contributing to measured bulk discharges and thus measured self-potential data are not
422 therefore expected to be a major hindrance to future applications of the self-potential method
423 to snow problems. We have also shown that with the exception of the zeta potential,
424 sensitivity to uncertainties in the snow properties governing the relationship between self-
425 potential data and liquid water contents are small (~ 3-4% in our feasibility study). Future
426 work must ascertain to what extent longer-term monitoring studies are affected by the
427 preferential elution of ions and the associated impacts on meltwater pH, EC and thus the zeta
428 potential. Even if such effects were found to be of concern, meltwater EC and pH are readily
429 monitored in-situ with automated probes and could be measured alongside self-potential data
430 at a calibration location, and subsequently be assimilated in snow models.

431 The final consideration focused on the assumption that the spatial pattern of self-
432 potential magnitudes, measured during the day across our survey areas, was due to temporal

changes in the liquid water content of the snowpack. This assumes that any spatial pattern due to elevation changes between the bottom and top of our survey areas is comparatively small and indeed negligible. Kulessa et al. (2003a) showed that elevation-driven changes in the self-potential fields measured between upstream (Ψ_{up}) and downstream (Ψ_{down}) locations (z_{up}, z_{down}) can be approximated by

$$\psi_{up} - \psi_{down} = -\frac{\xi'}{\eta\sigma_w} S_w \left(z_{up} - z_{down}\right), \tag{10}$$

here translated to our notation and adjusting for meltwater saturation according to equation (2). Even for the maximum daily values of saturation inferred from our measurements the elevation-driven spatial pattern has small magnitudes, estimated to be ~ -16.0 mV and -8.4 mV respectively for Jungfraujoch Glacier and Rhone Glaciers. These values are an order of magnitude smaller than daily changes measured at the two glaciers (Fig. 2) and are therefore considered to be insignificant for the purpose of the present feasibility study. In similar future applications the relevance of such spatial changes should be assessed on a case by case basis, and would in fact readily be incorporated into quantitative inferences of snow properties from self-potential data where they are of concern.

Overall our findings imply that in principle, self-potential data could be inverted for spatial or temporal variations in any one desired parameter (i.e. discharge, liquid water content, permeability or water chemistry), if independent estimates of the respective remaining parameters are available. Self-potential data are therefore well suited for assimilation in snow models along with meteorological and snowpack observations. We have shown in previous cryospheric applications that self-potential monitoring is readily effected with autonomous arrays of low-cost non-polarising electrodes connected to a high-impedance data logger (Kulessa et al., 2003a, 2003b, 2012). In operational practice for instance, 2-D

vertical arrays of electrodes and data loggers could be installed along with meteorological stations and upward-looking radar instrumentation, where the latter is used to monitor snow structure and 1-D liquid water contents. Assimilation of self-potential data along with complementary meteorological and radar data could then facilitate unique insights into daily and longer-term variations in 2-D vertical, lateral and preferential meltwater flows, or in liquid water contents. We conclude that the integration of self-potential measurements into existing snow measurement and data assimilation routines shows considerable promise in supporting a reduction of uncertainty in quantifying snow-atmosphere energy exchanges, or in predictive modelling used in operational snow forecasting.

Acknowledgements

This work was carried out while SST was working at VAW ETH Zurich within the Swiss National Science Foundation project; Accelerated release of persistent organic pollutants (POPs) from Alpine glaciers, Research Grant 200021_130083/1 BAFU, with support of the Swiss Federal Office for the Environment (FOEN/BAFU). We would like to thank two anonymous reviewers whose comments improved clarity of the manuscript and Martin Funk and VAW for hosting and supporting the work and for extensive support for fieldwork. Also thanks to Fabian Wolfsperger at WSL-Insititute for Snow and Avalanche Research SLF and Ludovic Baron at UNIL Université de Lausanne for providing equipment for fieldwork. Thanks to Jordan Mertes, Celia Lucas, Saskia Grindreaux, Barbara Reyes-Trüssel and Moira Thompson for invaluable help in the field.

References

Barnett, T.P., Adam, J.C., and Lettenmaier, D.P.: Potential impacts of a warming climate on water availability in snow-dominated Regions, Nature, 438(17), 303-309, doi: 10.1038/nature04141, 2005.

Campbell, F.M.A., Nienow, P.W., and Purves, R.S.: Role of the supraglacial snowpack in mediating meltwater delivery to the glacier system as inferred from dye tracer investigations, Hydrol. Process., 20(4), 969-985, doi: 10.1002/hyp.6115, 2006.

Colbeck, S.C., Akitaya, E., Armstrong, R., Gubler, H., Lafeuille, J., Lied, K., McClung, D., and Morris, E.: The International Classification for Seasonal Snow on the Ground: The International Commission on Snow and Ice of the International Association of Scientific Hydrology, 1990.

Corry, C.E., De Moully, G.T. and Gerety, M.T.: Field Procedure Manual for Self-Potential Surveys, Zonge Engineering and Research Organization Publishing, Arizona USA, 1983.

Darnet, M., Marquis, G., and Sailhac, P.: Estimating aquifer hydraulic properties from the inversion of surface streaming potential (SP) anomalies, Geophys. Res. Lett., 30(13), 1679, doi: 10.1029/2003GL017631, 2003.

Denoth, A.: An electronic device for long-term snow wetness recording, Ann. Glaciol., 19, 104-106, 1994.

Doherty, R., Kulessa, B., Ferguson, A.S., Larkin, M.J., Kulakov, L.A., and Kalin, R.M.: A microbial fuel cell in contaminated ground delineated by electrical self-potential and normalized induced polarization data, J. Geophys. Res., 115, G00G08, doi: 10.1029/2009JG001131, 2010.

Drzymala, J., Sadowski, Z., Holysz, L., and Chibowski, E.: Ice/water interface: Zeta potential, point of zero charge, and hydrophobicity, J. of Colloid Interf. Sci. 200, 229-243, 1999.

507 Essery, R., Morin, S., Lejeune, Y., and Ménard C.B.: A comparison of 1701 snow models
508 using observations from an alpine site, Adv. Water Resour. 55, 131-148, doi:
509 10.1016/j.advwatres.2012.07.013, 2013.
510 Fierz, C., Armstrong, R.I., Durand, Y., Etchevers, P., Greene, E., McClung, D.M.,
511 Nishimura, K., Satyawali, K., and Sokratov, S.A.: The International Classification for
512 Seasonal Snow on the Ground. IHP-VII Technical Documents in Hydrology N°83, IACS
513 Contribution N°1, UNESCO-IHP, Paris, 2009.
514 French, H. K., Binley, A., Kharkhordin, I., Kulessa, B. and. Krylov, S.S.: Permafrost and
515 snowmelt, in Applied Hydrogeophysics, Vereecken H. et al. (eds), 195–232, Springer, New
516 York, 2006.
517 Heilig, A., Eisen, O., and Schneebeli, M.: Temporal observations of a seasonal snowpack
518 using upward-looking GPR, Hydrol-Process, 24(22), 3133-3145, doi:10.1002/hyp.7749,2010.
519 Jouniaux, L., Maineult, A., Naudet, V., Pessel, M. and Sailhac, P.: Review of self-potential
520 methods in hydrogeophysics, C. R. Geoscience 341(10-11), 928-936, doi:
521 10.1016/j.crte.2009.08.008, 2009.
522 Kallay, N., Cop, A., Chibowski, E., and Holysz, L.: Reversible charge of ice-water interface,
523 II: Estimation of equilibrium parameters. J. Colloid Interf. Sci., 259, 89-96, doi:
524 10.1016/S00219797(02)00179-0, 2003.
525 Kulessa, B. A critical review of the low frequency electrical properties of ice sheets and
526 glaciers, JEEM 12(1), 23-36, doi: 10.2113/JEEG12.1.23, 2007.
527 Kulessa, B., Hubbard, B.P., and Brown, G.: Cross-coupled flow modelling of coincident
528 streaming and electrochemical potentials, and application to subglacial self-potential (SP)
529 data, J. Geophys. Res., 108(B8), 2381, doi: 10.1029/2001JB001167, 2003a.
530 Kulessa, B., Hubbard, B.P., and Brown, G.: Earth tide forcing of glacier drainage, Geophys.
531 Res. Lett., 30(1), doi: 10.1029/2002GL015303, 2003b.

Kulessa, B., Chandler, D.C., Revil, A., and Essery, R. L. H.: Theory and numerical modelling of electrical self-potential (SP) signatures of unsaturated flow in melting snow, Water Resour. Res. 48, W09511, doi: 10.1029/2012WR012048, 2012.

Linde, N., Revil, A., Bolève, A., Dagès, C., Castermant, J., Susli, B. and Voltz, M.: Estimation of the water table throughout a catchment using self-potential and piezometric data in a Bayesian framework, J. of Hydrol. 334, 88-98, doi: 10.1016/j.jhydrol.2006.09.027.

Livneh, B., Xia, Y., Mitchell, K.E., Ek, M.B., and Lettenmaier, D.P.: Noah LSM Snow Model Diagnostics and Enhancements, J. Hydrometeorol., 11, 721–738, doi: 0.1175/2009JHM1174.1, 2010.

Meyer, T. and Wania, F.: Organic contaminant amplification during snow melt, Water Res. 42(8-9), 1847-1865, doi:10.1016/j.watres.2007.12.016, 2008.

Meyer, T., Lei, Y.D. and Wania, F.: Organic contaminant release from melting snow. 1. Influence of chemical partitioning, Environ. Sci. Technol. 43(3), 657-662, doi: 10.1021/es8020217, 2009.

Mitterer, C., Heilig, A., Schweizer, J., and Eisen, O.: Upward-looking ground-penetrating radar for measuring wet-snow properties, Cold Reg. Sci. Technol., 69(2-3), 129-138, doi: 10.1016/j.coldregions.2011.06.003. 2011.

Petiau, G.: Second generation of lead-lead chloride electrodes for geophysical applications, Pure and Appl. Geophys., 157(3), 357-382, doi: 10.1007/s000240050004, 2000.

Revil, A., Schwaeger, H., Cathles, L.M. and Manhardt, P.: Streaming potential in porous media. II: Theory and application to geothermal systems, J. Geophys. Res., 104, 20,033–20,048, doi: 10.1029/ 1999JB900090, 1999.

Revil, A., Naudet, V., Nouzaret, J., and Pessel, M.: Principles of electrography applied to self-potential elecrokinetic sources and hydrogeological application, Water Resour. Res., 39(5), 1-14, doi: 10.1029/2001WR000916, 2003.

Revil, A., Titov, K., Doussan, C., and Lapenna, V.: Application of the self-potential method to hydrological problems, in: H. Vereecken, A. Binley, G. Cassiani, A. Revil, and K. Titov (eds.), Applied Hydrogeophysics, Springer, Netherlands, 255-292, 2006.

Revil, A., Linde, N., Cerepi, A., Jougnot, D., Matthäi, S. and Finsterle, S.: Electrokinetic coupling in unsaturated porous media, J. of Colloid Interf. Sci. 313(1), 315-327, doi: 10.1016/j.jcis.2007.03.037, 2007.

Schmid, L., Heilig, A., Mitterer, C., Schweizer, J., Maurer, H., Okorn, R., and Eisen, O.: Continuous snowpack monitoring using upward-looking ground-penetrating radar technology, J. Glaciol., 60(221), 509-525, doi: 10.3189/2014JoG13J084, 2014.

Shimizu, H.: Air permeability of deposited snow. Low Temperature Science Series A 22, 1-32, 1970.

Sill, W.R.: Self-potential modeling from primary flows, Geophysics 48, 76–86, doi: 10.1190/1.1441409, 1983.

Thompson, S.S., Kulessa, B. and Luckman, A.: Integrated electrical resistivity tomography (ERT) and self-potential (SP) techniques for assessing hydrological processes within glacial lake moraine dams, J. Glaciol., 58 (211), 1-10, doi: 10.3189/2012JoG11J235, 2012.

Wever, N., Fierz, C., Mitterer, C., Hirashima, H. and Lehning, M.: Solving the Richards Equation for snow improves snowpack meltwater runoff estimations in detailed multi-layer snowpack model, The Cryosphere, 8(1), 257-274, doi: 10.5194/tc-8-257-2014, 2014.

Williams, M.W., Cline, D., Hartman, M. and Bardsley, T.: Data for snowmelt model development, calibration and verification at an alpine site, Colorado Front Range, Water Resour. Res. 35 (10), 3205-3209, doi: 10.1029/1999WR900088, 1999.

Williams, M. W., Erickson, T. A., and Petrzelka, J. L.: Visualising meltwater flow through snow at the centimetre-to-metre scale using a snow guillotine, Hydrol. Process. 24 (15), 2098-2110, doi: 10.1002/hyp.7630, 2010.

582 **TABLES AND FIGURES**

583

584 **Table 1:** Best estimate of each parameter for Rhone Glacier SP (Day 2) and relative assumed
585 uncertainty and sensitivity ranges. The sensitivity ranges are based on the measurement
586 accuracy of each measured parameter or the confidence of estimates parameters. The
587 uncertainty ranges are exaggerated from the sensitivity values to highlight the effect of poor
588 measurement or estimation. .

589

Measured / estimated parameters	**Best estimate**	**Uncertainty range**	**Sensitivity range**
Self-potential ψ_m (V)	Variable	$\psi_m \pm 40\%$	$\psi_m \pm 20\%$
Discharge Q ($m^3 s^{-1}$)	Variable	$Q \pm 40\%$	$Q \pm 20\%$
Electrical conductivity σ_w ($S m^{-1}$)	5×10^{-6}	$10^{-7} – 10^{-4}$	$\sigma_w \pm 5 \times 10^{-7}$
Zeta potential ζ (V)	-1×10^{-5}	$10^{-4} – 10^{-6}$	$\zeta \pm 50\%$
Permeability from;			
Grain diameter d (m)	0.00175	$d \pm 0.001$	$d \pm 0.0005$
Density ρ ($kg m^3$)	555.5	$\rho \pm 140$	$\rho \pm 70$
Cross sectional area from;			
Width w (m)	12.5	$w \pm 10$	$w \pm 5$
Depth dp (m)	1.45	$dp \pm 1$	$dp \pm 0.2$

590

591

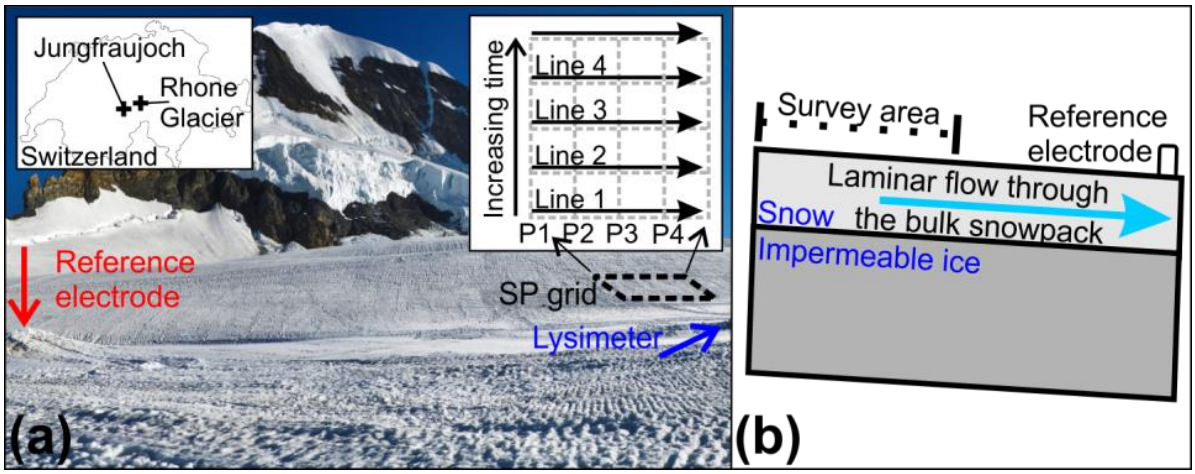

Figure 1: (a) Example survey set up. Insert left show the location of both fieldsites. Insert right illustrates the self-potential survey design; to provide each self-potential data value, a profile of 25 data points (P1, P2, etc.) was collected (Line 1, Line 2, etc.), perpendicular to assumed bulk water flow. (b) Schematic of the self-potential experiment developed by Kulessa et al. (2012) for the situ snowpack surveys.

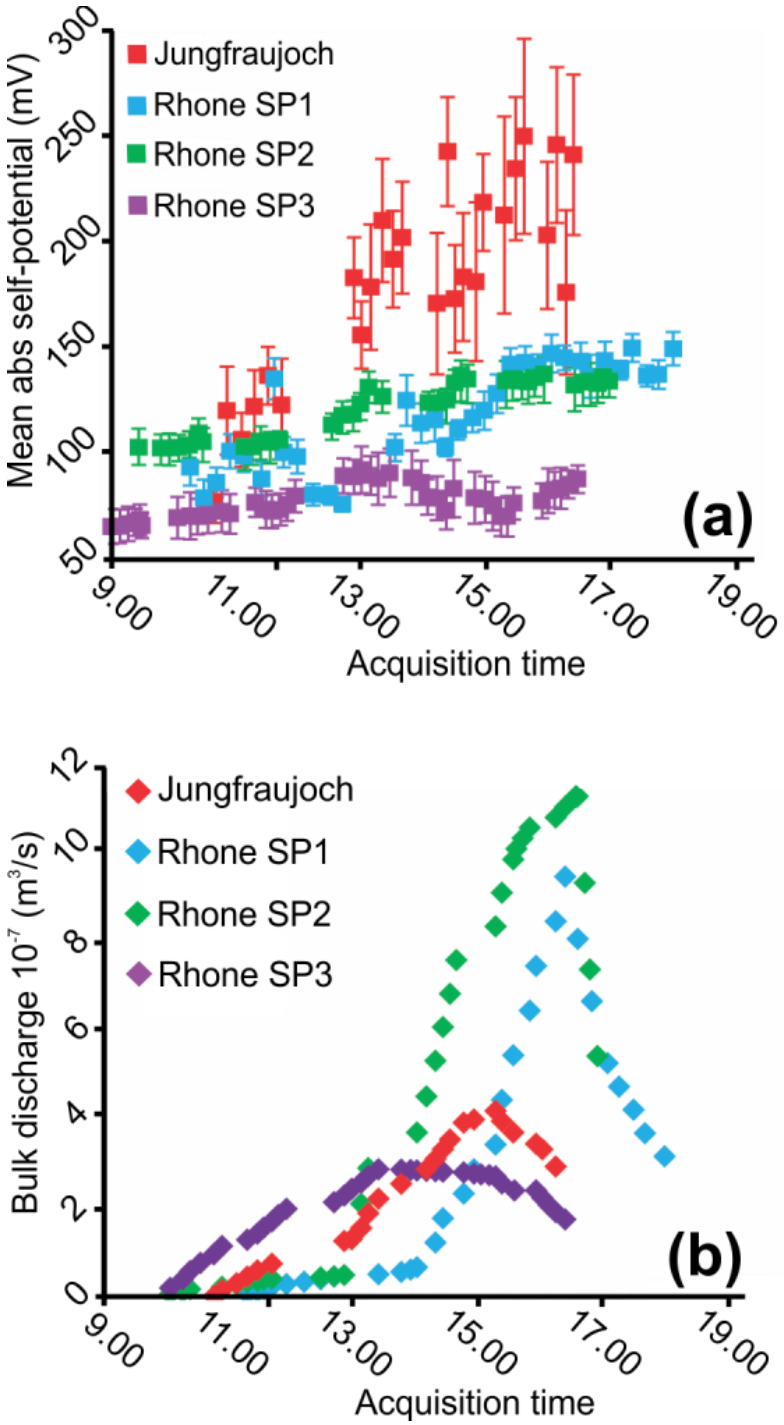

600

601 **Figure 2:** Time series of (a) bulk self-potential measurements and (b) bulk discharge
602 measurements for the three Rhone Glacier surveys and the Jungfraujoch Glacier survey. Each
603 self-potential data point represents the mean value of a profile (consisting of 25 data points);
604 the error bars illustrates the variability over each profile. Bulk discharge was measured over
605 each profile by the lysimeter.

606

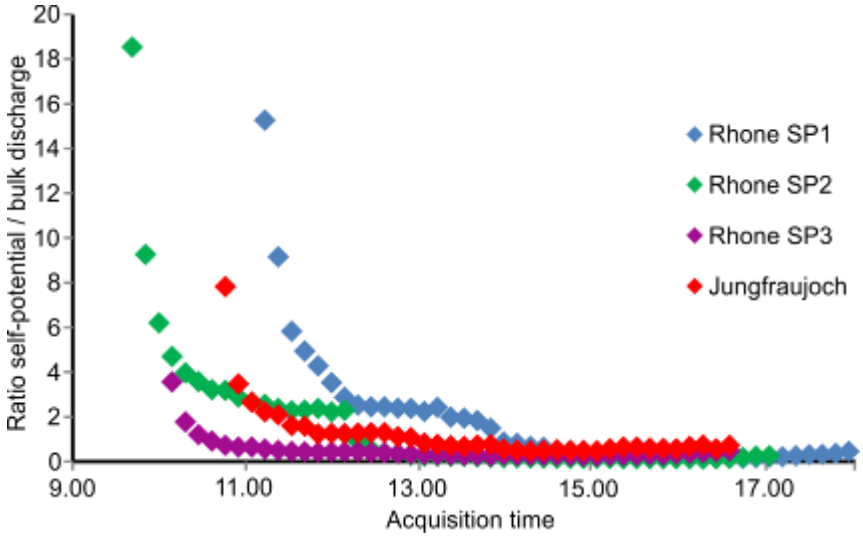

Figure 3: Ratio between self-potential (V) and bulk discharge (m^3 s^{-1}) for each of the four surveys through time, illustrating the ratio changes consistently over time.

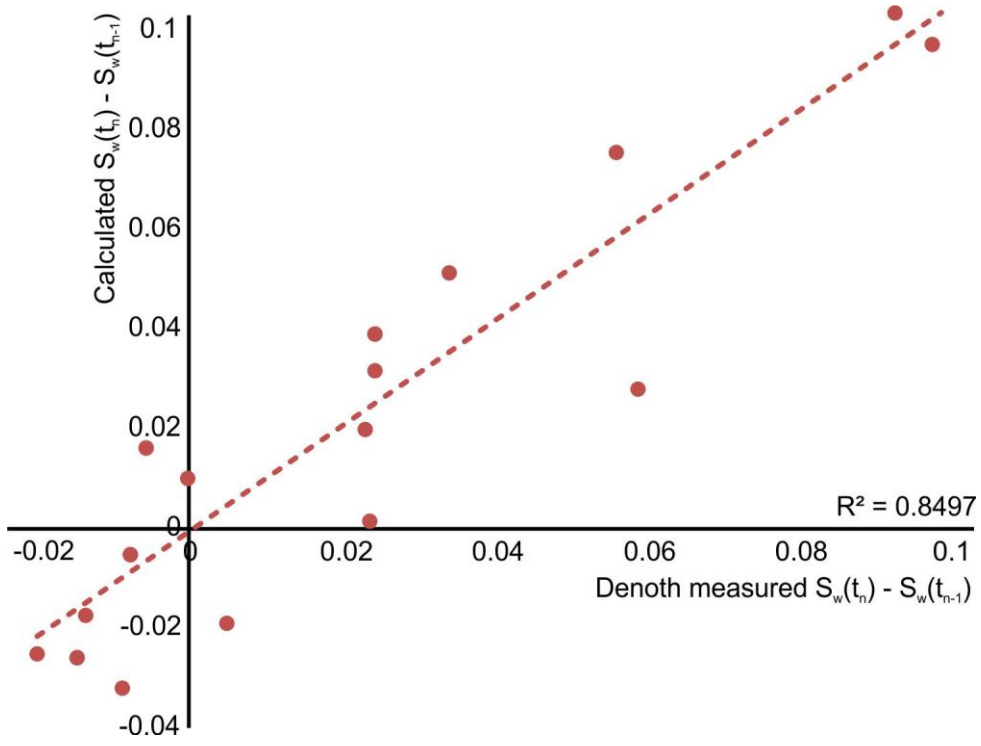

Figure 4: Temporal differences in S_w inferred from self-potential data against temporal differences in the Denoth measured S_w at Jungfraujoch Glacier, according to equation (5).

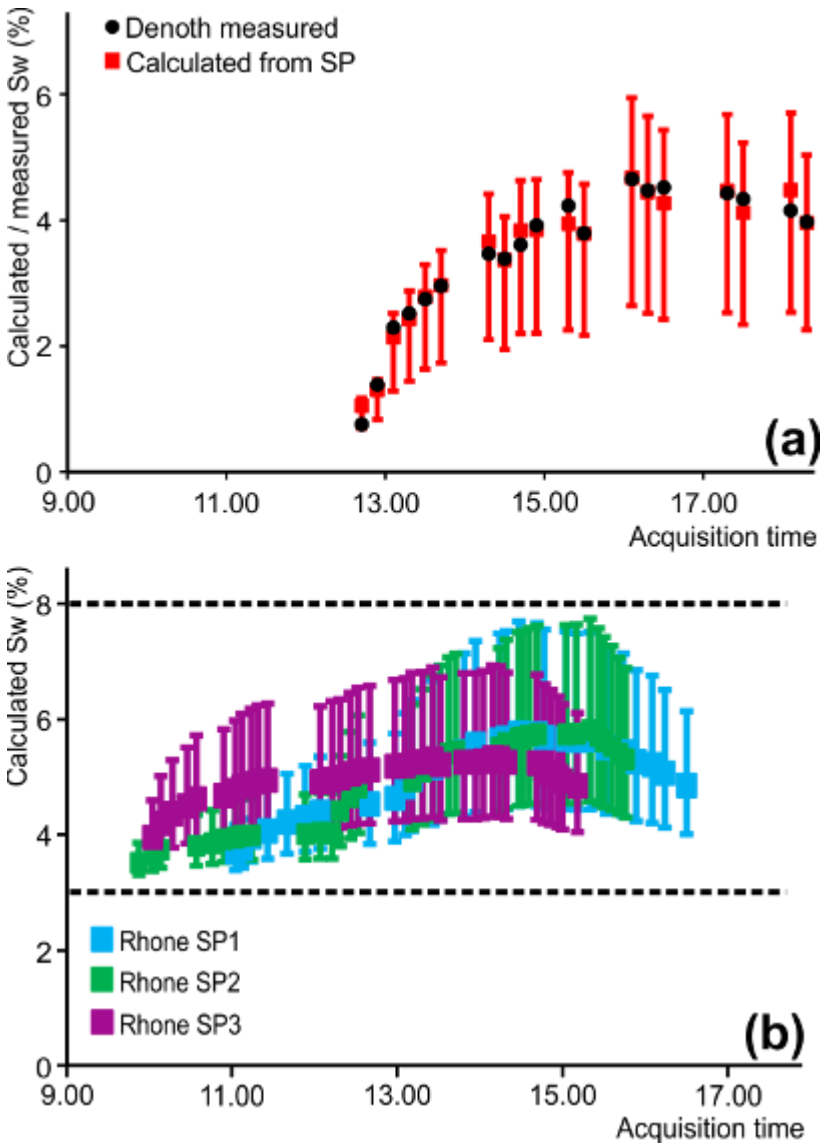

Figure 5: (a) Liquid water content calculated from equation 4 for the self-potential survey carried out at Jungfraujoch Glacier, with the corresponding Denoth measurements. The uncertainty range illustrates the minimum and maximum model results for the range of parameters (Table 1, Supplementary Material). (b) Liquid water content calculated from equation 4 for each of the three self-potential surveys carried out at Rhone GlacierAll results are within the range of liquid water content (% vol) estimated by the hand tests (black dashed lines in b).

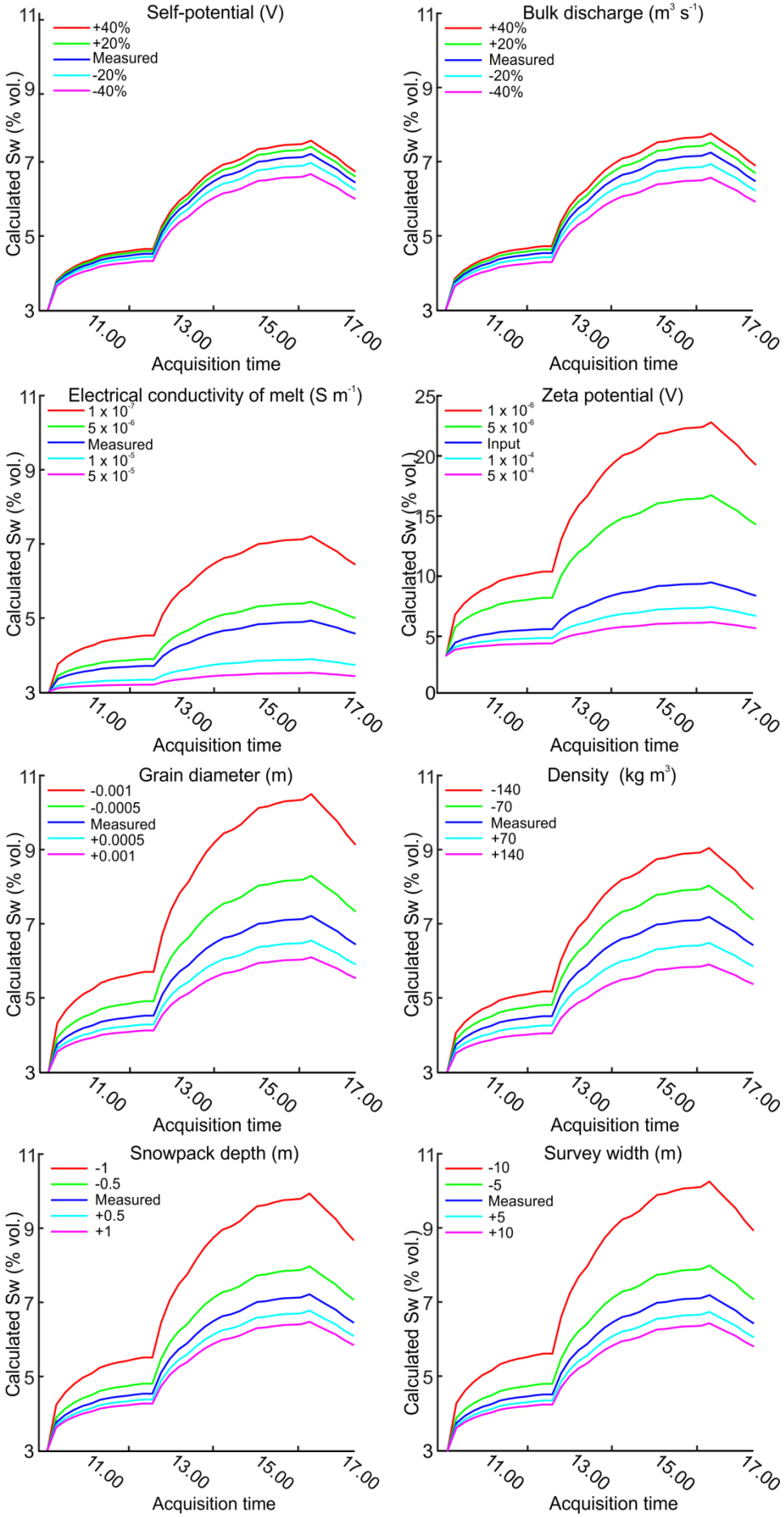
Self-potential (V)
+40%
+20%
Measured
-20%
-40%
Bulk discharge (m3 s-1)
Electrical conductivity of melt (S m-1)
1 x 10-7
5 x 10-6
1 x 10-5
5 x 10-5
Zeta potential (V)
1 x 10-6
5 x 10-6
Input
1 x 10-4
5 x 10-4
Grain diameter (m)
-0.001
-0.0005
+0.0005
+0.001
Density (kg m3)
-140
-70
+70
+140
Snowpack depth (m)
-1
-0.5
+0.5
+1
Survey width (m)
-10
-5
+5
+10
Calculated Sw (% vol.)
Acquisition time
11.00
13.00
15.00
17.00

624

Figure 6: S_w calculations for a range of values for each parameter. In each case the range is an exaggerated uncertainty range (Table 1), highlighting the effect of each individual parameter on the calculated S_w output, using Rhone Glacier SP2 as an example.

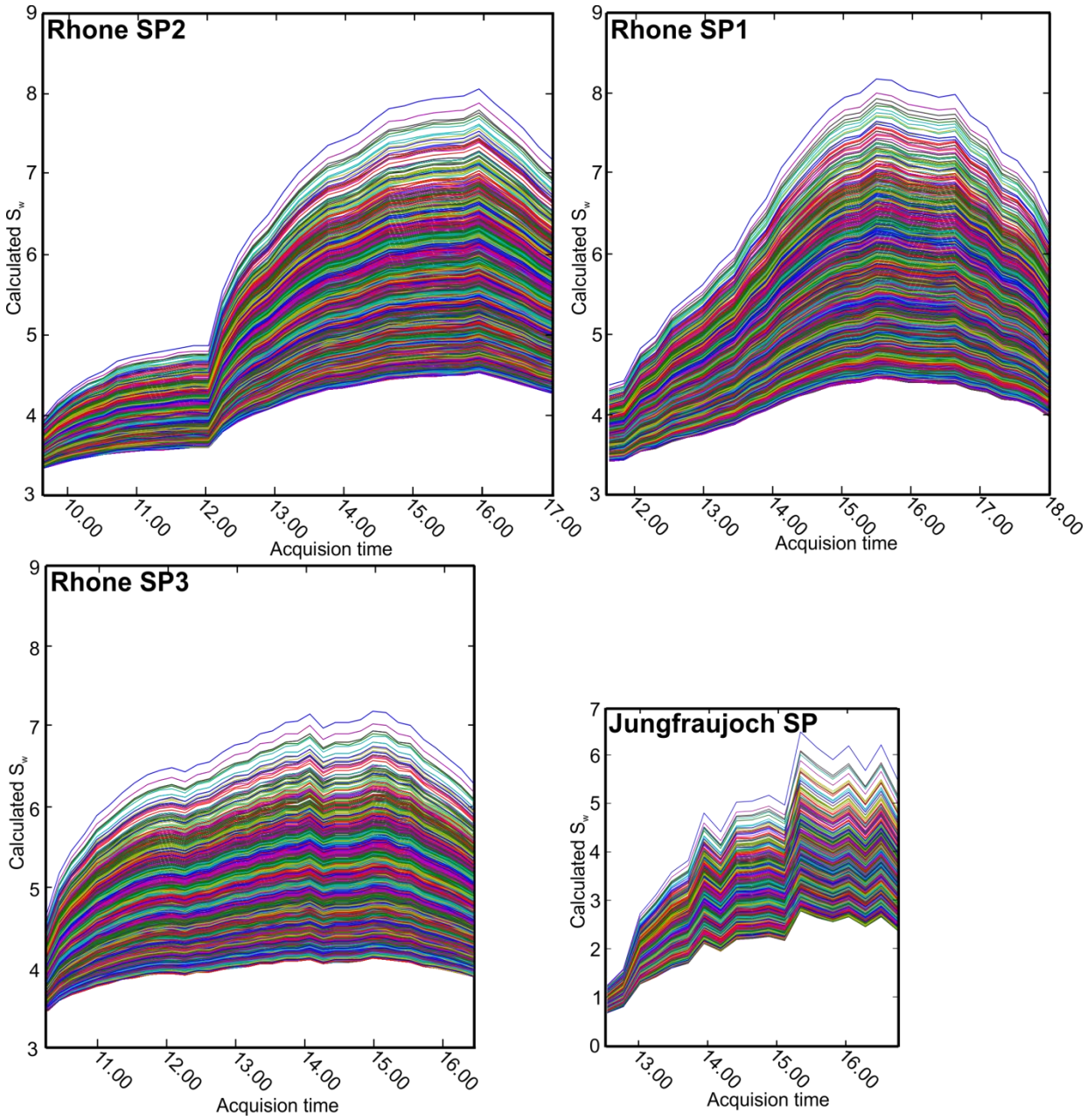

Figure 7: Full sensitivity analysis for each of the four data sets. Each graph shows the full range of calculated liquid water content (S_w) values of every combination of minimum, best estimate and maximum for each of the parameters.